Talanta 81 (2010) 339–345

Contents lists available at ScienceDirect

Talanta

journal homepage: www.elsevier.com/locate/talanta

In situ growth of copper sulfide nanoparticles on ordered mesoporous carbon and their application as nonenzymatic amperometric sensor of hydrogen peroxide

Xiangjie Bo, Jing Bai, Lixia Wang, Liping Guo*

Faculty of Chemistry, Northeast Normal University, Renmin Street 5268, Changchun 130024, Jilin, PR China

ARTICLE INFO

Article history:
Received 27 September 2009
Received in revised form 4 December 2009
Accepted 9 December 2009
Available online 16 December 2009

Keywords:
Copper sulfide
Ordered mesoporous carbon
Nonenzymatic sensor
Hydrogen peroxide
In situ growth

ABSTRACT

A simple and facile synthetic method to incorporate copper sulfide (Cu_2S) nanoparticles inside the mesopores of ordered mesoporous carbons (OMCs) is reported. The Cu_2S/OMCs nanocomposite was characterized by transmission electron microscopy (TEM), X-ray diffraction (XRD), X-ray photoelectron spectroscopy (XPS), and nitrogen adsorption–desorption. The results show that the incorporation of Cu_2S nanoparticles inside the pores of OMCs does not change the highly ordered two-dimensional hexagonal mesostructure of OMCs matrix. Nonenzymatic amperometric sensor of hydrogen peroxide based on the Cu_2S/OMCs nanocomposite modified glassy carbon (GC) electrode is developed. Compared with the pristine OMCs modified electrode, the Cu_2S/OMCs modified electrode displays high electrocatalytic activity towards hydrogen peroxide and gives linear range from 1 to 3030 μM (R = 0.9986). The sensor also exhibits good ability of anti-interference to electroactive molecules. The combination of the unique properties of Cu_2S nanoparticles and the ordered mesostructure of OMCs matrix guarantee the excellent electrocatalysis for hydrogen peroxide. The good analytical performance and low-cost make Cu_2S/OMC nanocomposite promising for the development of effective sensor for hydrogen peroxide.

© 2009 Elsevier B.V. All rights reserved.

1. Introduction

Since the discovery of the OMCs by Ryoo et al. [1], a great deal of effort has been devoted to the fundamental research and applications of OMCs. The unique ordered structure and the remarkable physical–chemical properties of OMCs, such as periodic mesoporous structure, high specific surface area, large pore volume, and chemical inertness, have made them widely usable in electrocatalytic applications [2–11]. The functionalization of the surface and pores of OMCs with a variety of organic and inorganic species permits the fabrication of novel hybrid materials. Many novel strategies used to alter the physical properties of OMCs have been reviewed by Stein et al. [12] and Dai et al. [13], respectively. Among these surface modifications, the linkage of nanoparticles to OMCs extends the applications of OMCs-based hybrid nanomaterials [14–18]. Cu_2S is a p-type semiconductor with a bulk band gap of 1.2 eV and has wide applications as materials for solar cells [19], cold cathodes [20], electrochemical sensor [21], and nanoscale switches [22]. There have been reports about direct thermal growth of Cu_2S nanocrystals on carbon nanotubes (CNTs) [19,21]. However, the Cu_2S nanocrystals only cover the outer surface of CNTs and the surface of the CNTs often must be functionalized to increase the hydrophilicity, which probably impacts the performance of the resulting hybrid nanomaterials. Several types of metal sulfide such as CdS [23–27], ZnS [28,29], and PbS [30] have been prepared inside the mesopores of ordered mesoporous silica materials. Due to the semiconductivity of ordered mesoporous silicas, they are not favorable for applications in electrode materials. Therefore, it is highly desirable to disperse metal sulfide catalysts on electronically conductive support to reduce ohmic resistance and facilitate charge transfer for electrochemical applications. Here we report a simple method to embed Cu_2S nanoparticles inside the pores of OMCs. The nanosized mesopores of OMCs can be used as nanoreactors for growth of nanoparticles, while the accessible ordered pores can provide sufficient room for mass transport. The combination of the two components brings together the advantages of high surface area of OMCs and unique properties of Cu_2S nanoparticles, which endows the excellent electrocatalytic activity of Cu_2S/OMCs hybrid materials.

Hydrogen peroxide has wide applications in environmental, pharmaceutical, clinical, and industrial research. It is also a by-product of the reaction catalyzed by large number of oxidase enzymes. Therefore the detection of hydrogen peroxide is important in biomedical and environmental applications. Several analytical methods have been developed to detect the hydrogen peroxide, including chemiluminescence [31,32], fluorimetric method [33], and spectrophotometry [34]. Compared with these approaches, electrochemical sensors are of particular interest for their practicality, simplicity, low-cost, and suitability for real-time detection. Enzyme or protein modified electrodes have been

* Corresponding author. Tel.: +86 0431 85099762; fax: +86 0431 85099762.
E-mail address: guolp078@nenu.edu.cn (L. Guo).

0039-9140/$ – see front matter © 2009 Elsevier B.V. All rights reserved.
doi:10.1016/j.talanta.2009.12.007

usually used as amperometric biosensors of hydrogen peroxide. Various immobilizing matrices, especially nanomaterials, have been used to construct the enzyme or protein biosensors, such as CNTs [35–38], ordered mesoporous materials [39–43], and metal oxides [44–46]. Although these biosensors show high selectivity and sensitivity, the wide application of enzyme or protein biosensors is hindered by the thermal and chemical instabilities of the enzymes or proteins. Also, the immobilized enzymes or proteins are relatively expensive. To overcome the obstacle, increasing attention has been focused on the nonenzymatic biosensors, such as Fe_3O_4 nanoparticles [47], Ag nanomaterials [48,49], and Cu_2O microcubes [50]. There have been reports about the direct electrocatalytic reduction of hydrogen peroxide at Fe_3O_4 nanoparticles [51] and Prussian Blue [52] film decorated OMCs modified electrode. But few works are available on hydrogen peroxide detection at Cu_2S/OMCs nanocomposite modified electrode.

In this work, we introduce a simple in situ method to incorporate Cu_2S nanoparticles inside the pores of OMCs. Hydrogen peroxide was selected as marked molecule to evaluate the electrocatalytic activity of this new hybrid nanocomposite. The improvement of the electrocatalytic property of Cu_2S/OMCs is observed in comparison with pristine OMCs.

2. Experimental

2.1. Reagents and apparatus

Pluronic P123 (non-ionic triblock copolymer, $EO_{20}PO_{70}EO_{20}$), and Nafion (5 wt%) were purchased from Sigma–Aldrich. Dodecanethiol ($C_{12}H_{25}SH$), thioacetamide (TAA), cuprous chloride (CuCl), and hydrogen peroxide 30% (w/w) were obtained from Beijing Chemical Co. (China). All other reagents used were of analytical grade and used as received without further purification. The 0.1 M phosphate buffered saline (PBS, pH 7.3) was employed as supporting electrolytes for electrocatalysis of hydrogen peroxide.

Cyclic voltammogram (CV), electrochemical impedance spectroscopy (EIS), and chronoamperometry (CA) were performed on a CHI660C electrochemical workstation (CH Instruments, China) connected to a personal computer. A three-electrode configuration was employed, consisting of GC electrode (3 mm diameter) or a modified GC electrode serving as a working electrode, whereas an Ag/AgCl (in saturated KCl solution) and a platinum wire served as the reference and counter electrodes, respectively. XRD patterns were obtained on an X-ray D/max-2200vpc (Rigaku Corporation, Japan) instrument operated at 40 kV and 20 mA and using Cu Kα radiation (k = 0.15406 nm). Nitrogen adsorption–desorption isotherms were performed on ASAP 2020 (Micromeritics, USA). The specific surface area was calculated by the Brunauer–Emmett–Teller (BET) method. The pore size was obtained from the adsorption branch of the isotherm by the Barrett–Joyner–Halenda method. The total pore volume was determined from the amount of liquid N_2 adsorbed at a relative pressure of about 0.99. TEM images were obtained using a JEM-2100F transmission electron microscope (JEOL, Japan) operating at 200 kV. XPS was measured using Thermo ESCA LAB spectrometer (USA).

2.2. Synthesis of OMCs and Cu_2S/OMCs

The silica templates (SBA-15) were synthesized using Pluronic P123 as the surfactant and tetraethyl orthosilicate as the silica source [53]. OMCs were prepared according to the method reported by Ryoo et al. [54].

The preparation of Cu_2S/OMCs is schematically presented in Scheme 1. Cu_2S/OMCs were synthesized by the following procedure: 110 mg of OMCs was dispersed in 150 mL of diethyl ether absolute containing 50 mg CuCl. After mild ultrasonication for 5 h and stirring for 1 day in a sealed vial at room temperature, the CuCl could diffuse into the pores of OMCs. Then the resultant sample was dried under vacuum to give a fine and completely dry powder. 10 mL $C_{12}H_{25}SH$ was added to the resultant sample and then heated to 120 °C. A warm solution (~90 °C) of 10 mL $C_{12}H_{25}SH$ including 0.1 g TAA was added into the above solution, then aged at 100 °C for 10 h. The precipitate was collected by centrifugation and washed with hot ethanol several times to remove the excess $C_{12}H_{25}SH$. The product was collected and dried in an oven at 80 °C.

2.3. Fabrication of modified electrode

Approximately 60 min of ultrasonication was necessary to disperse 5 mg Cu_2S/OMCs into a mixture of 0.2 mL (5 wt%) Nafion and

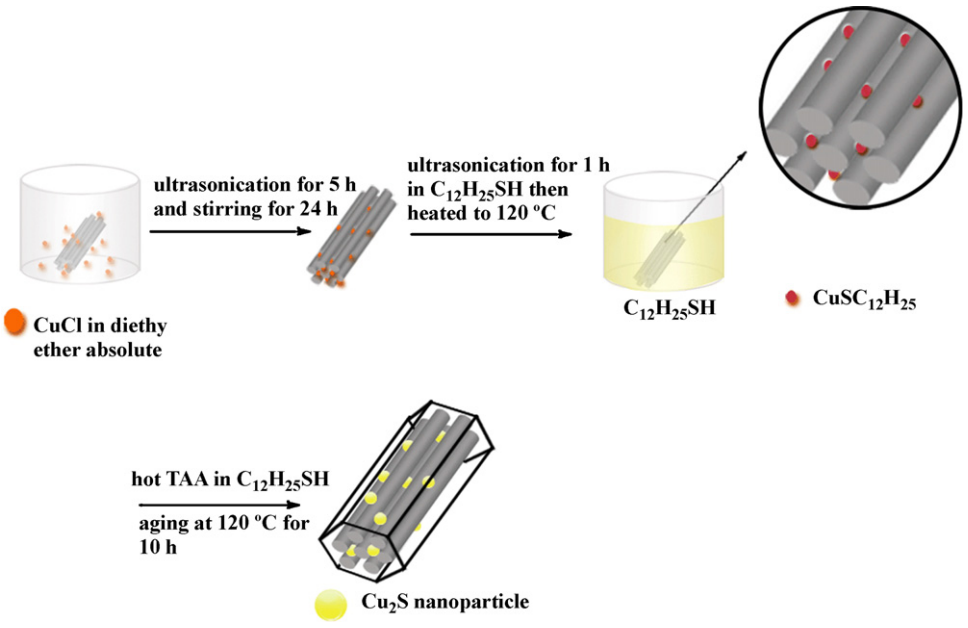

Scheme 1. Illustration of the preparation of Cu_2S/OMCs nanocomposite.

1.8 mL distilled water. After dropping 5 μL of the suspension on the electrode surface, the electrode was dried in air.

3. Results and discussion

3.1. Characterization of Cu_2S/OMCs nanocomposite

The influence of incorporation of Cu_2S nanoparticles on the mesostructure of OMCs was investigated by XRD. Fig. 1A displays the typical small-angle XRD patterns of OMCs (a) and Cu_2S/OMCs (b). The synthesized OMCs are replicas of the parent templates SBA-15 [53], as it is evident from the presence of three XRD peaks at 2θ of 1.0°, 1.7°, and 2.0°. Three XRD peaks are observed with d spacings of 88, 51, and 44 Å, which implies that these three observed peaks can be indexed as (1 0 0), (1 1 0), and (2 0 0) diffraction peaks of mesoporous hexagonal space group $p6mm$. The existence of the main diffraction peak (1 0 0) illustrates that the framework hexagonal ordering of OMCs is basically retained after the incorporation of Cu_2S nanoparticles. The marked intensity decrease of Cu_2S/OMCs diffraction peaks is related to the in situ growth of Cu_2S nanoparticles inside the pores. The pore filling of the Cu_2S nanoparticles can reduce the scattering contrast between the pores and the walls of the mesoporous material [55]. Fig. 1B shows the wide-angle XRD patterns of OMCs (a) and Cu_2S/OMCs (b). Two broad diffraction peaks at 2θ of 23.4° and 44.5° are observed at OMCs sample, corresponding to the (0 0 2) and (1 0 1) diffractions of graphite. However, several peaks appear in the wide-angle XRD pattern of Cu_2S/OMCs nanocomposite, which can be ascribed to the characteristic peaks of Cu_2S (JCPDS84-206), which confirms the formation of Cu_2S/OMCs nanocomposite.

Fig. 1C presents the nitrogen adsorption–desorption isotherms of OMCs (a) and Cu_2S/OMCs (b). The resulting sorption isotherms are all type IV isotherms with a pronounced capillary condensation step, characteristic of high-quality mesoporous materials. The presence of an H1 hysteresis loop indicates channel-like pores. It is observed that the isotherm changes considerably after in situ growth of Cu_2S nanoparticles inside the pores of OMCs. First, the adsorption capacity decreases after the incorporation of Cu_2S nanoparticles. Second, the shift of the capillary condensation step to lower relative pressure evidences a decrease of the pore size. The textural parameters of the OMCs and Cu_2S/OMCs obtained from the nitrogen adsorption measurements are summarized in Table 1. The BET surface areas for OMCs and Cu_2S/OMCs are calculated to be 903 and 587 m^2/g, respectively. The Cu_2S nanoparticles partially occupy the pores of OMCs and nitrogen molecules cannot access the surface of pores, and then the BET surface area of Cu_2S/OMCs decreases compared with OMCs matrix. The total pore volumes of OMCs and Cu_2S/OMCs are 1.07 and 0.69 cm^3/g, which also suggest that Cu_2S nanoparticles are embedded in the pore channels of OMCs.

Table 1
Textural parameters of OMCs and Cu_2S/OMCs nanomaterials.

Samples	D (nm)[a]	S_{BET} ($m^2\ g^{-1}$)[b]	V ($cm^3\ g^{-1}$)[c]
OMCs	3.7	903	1.07
Cu_2S/OMCs	2.3	587	0.69

[a] Pore diameter.
[b] BET surface area.
[c] Pore volume.

Fig. 1D shows the XPS Cu2p and S2p spectra for Cu_2S/OMCs nanocomposite. The peaks at 953.1 and 932.7 eV can be assigned to the excitations from the Cu2p1/2 and Cu2p3/2 core levels, respectively, which is in accordance with the literature [19]. The sulfur peak consists of a spin split doublet of S2p3/2 and S2p1/2; the binding energies of them correspond to 161.3 and 162.5 eV. This demonstrates the formation of Cu_2S/OMCs nanocomposite.

Fig. 2 exhibits typical TEM images of OMCs and Cu_2S/OMCs nanocomposite. TEM images of OMCs clearly show highly ordered carbon nanowires viewed from the [1 0 0] (A) and [0 0 1] (B) directions. The structure of OMCs is exactly an inverse replica of their mother mold SBA-15. Compared with the pristine OMCs, the pore channels are distorted to a certain degree after assembling Cu_2S nanoparticles (C), which reveals that Cu_2S nanoparticles are incorporated inside the pore channels. It can be seen that Cu_2S nanoparticles are uniformly dispersed in the pores of OMCs. But few Cu_2S nanoparticles aggregate with the size up to 30 nm, which

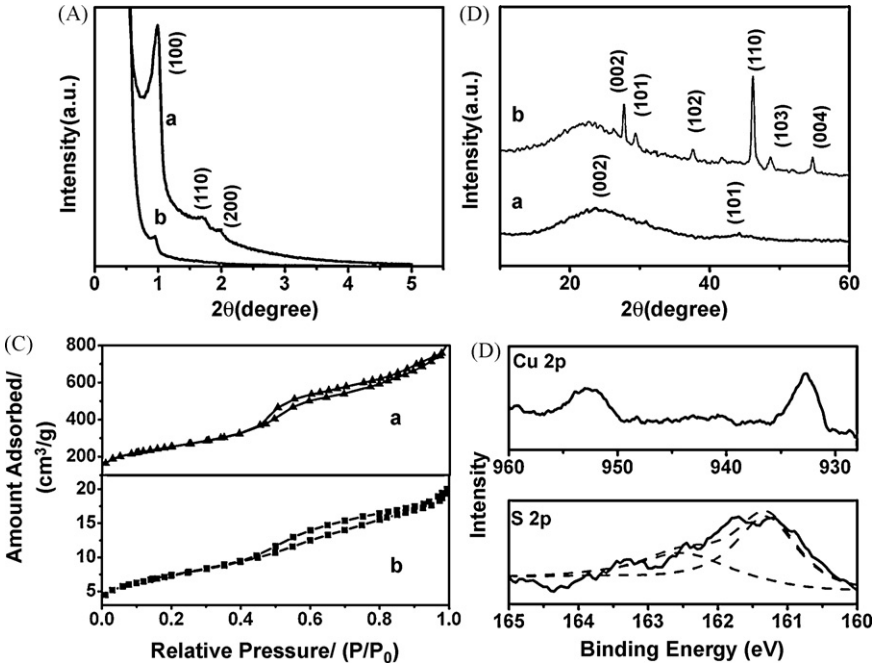

Fig. 1. (A) Small-angle XRD of (a) OMCs and (b) Cu_2S/OMCs nanocomposite. (B) Wide-angle XRD of (a) OMCs and (b) Cu_2S/OMCs nanocomposite. (C) Nitrogen adsorption–desorption isotherms for (a) OMCs and (b) Cu_2S/OMCs nanocomposite. (D) XPS of Cu2p and S2p of Cu_2S/OMCs nanocomposite.

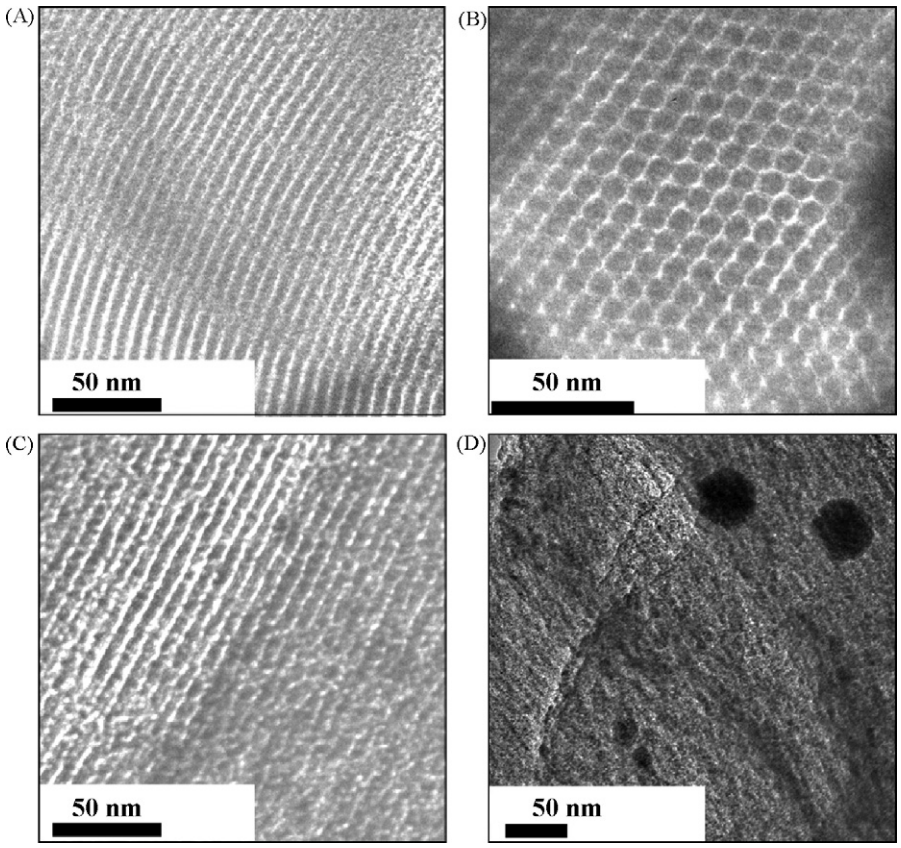

Fig. 2. (A) TEM image of OMCs viewed from [1 0 0]; (B) TEM image of OMCs viewed from [0 0 1] directions; and (C and D) TEM images of Cu_2S/OMCs nanocomposite.

is much larger than the pore size of OMCs, can be found on the outer surface rather than inside the pores (D).

EIS was applied to study impedance changes on the electrode surface of different modified electrodes. Fig. 3 exhibits the EIS results of four electrodes in 5 mM $Fe(CN)_6^{4-/3-}$ and 0.1 M KCl at +0.25 V. The EIS includes a semicircular part and a linear part. The semicircular part at higher frequencies corresponds to the electron transfer limited process, and the diameter is equivalent to the electron transfer resistance (Rct). After GC was modified with Nafion film (Fig. 3d), Rct increases markedly, perhaps due to the Nafion film acting as a barrier and blocking interfacial charge transfer.

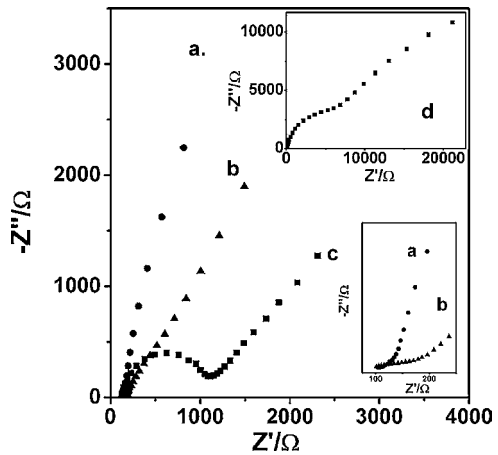

Fig. 3. EIS of (a) OMCs/Nafion/GC, (b) Cu_2S/OMCs/Nafion/GC, (c) GC and (d) Nafion/GC in 0.10 M KCl containing 5 mM $Fe(CN)_6^{3-/4-}$ solutions at +0.25 V from 0.1 Hz to 10.0 kHz. Inset shows the amplification of EIS of (a) OMCs/Nafion/GC and (b) Cu_2S/OMCs/Nafion/GC.

Compared with the GC electrode (Fig. 3c), a dramatical decrease of the diameter is observed at OMCs/Nafion/GC (Fig. 3a). This can be explained by the excellent conductivity of OMCs. When semiconductive Cu_2S nanoparticles were grown inside the pores of OMCs matrix, the diameter increases slightly (Fig. 3b), suggesting the Cu_2S/OMCs nanocomposite was successfully prepared.

CVs in Fig. 4A were used to investigate the electrocatalytic property of Cu_2S/OMCs/Nafion/GC. A pair of quasi-reversible redox peaks at −0.15 and −0.30 V is observed at the OMCs/Nafion/GC electrode (curve a), corresponding to the protonation/depronation of surface oxygen-containing functional groups [10]. Compared with OMCs/Nafion/GC electrode, the Cu_2S/OMCs/Nafion/GC electrode (curve b) exhibits a pair of well-defined redox peaks at −0.09 and +0.22 V in the blank PBS (pH 7.3), which are assigned to the Cu_2S/CuS redox couple, similar to Cu_2O/CuO [50]. And the peaks related to the protonation/depronation of surface oxygen-containing functional groups at −0.15 and −0.30 V is not obvious. It is clearly seen that the CVs of bared GC (curve c) or Nafion/GC (curve d) electrodes show low background current and glossy tracks, which indicated no electroactive substances exist on the electrode surface. Fig. 4B shows the CVs of Cu_2S/OMCs/Nafion/GC in 0.1 M PBS at different scan rates. The plots of peak current versus scan rate exhibit the peak currents increased linearly with square root of the scan rate in the range 10–600 mV s^{-1}. This means that the electrode process is controlled by diffusion.

3.2. Electrocatalytic reduction of hydrogen peroxide at different electrodes

Fig. 5 presents the CVs of OMCs/Nafion/GC, Cu_2S/OMCs/Nafion/GC, GC, and Nafion/GC in 0.1 M PBS (pH 7.3) in the presence and absence of hydrogen peroxide at 50 mV s^{-1}. Before experiments the PBS solution was degassed with nitrogen gas

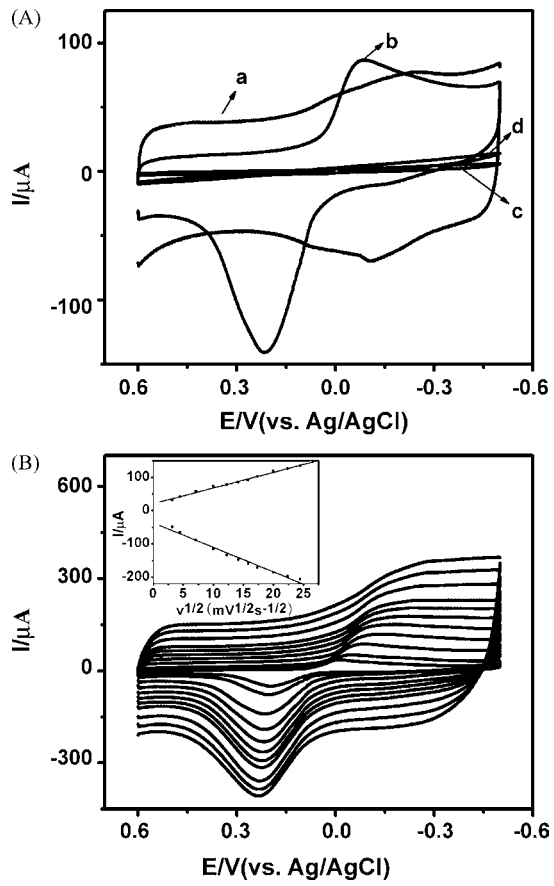

Fig. 4. (A) CVs of (a) OMCs/Nafion/GC, (b) Cu_2S/OMCs/Nafion/GC, (c) GC and (d) Nafion/GC in 0.1 M PBS (pH 7.3) at 50 mV s^{-1}. (B) CVs of Cu_2S/OMCs/Nafion/GC in 0.1 M PBS (pH 7.3) at scan rate of (from inner to outer): 10, 20, 50, 100, 150, 200, 250, 300, 400, 500 and 600 mV s^{-1}. Inset: the linear relationship between the peak currents and the square root of scan rates.

for 15 min. Upon the addition of 5 mM hydrogen peroxide, a broad peak at −0.31 V is observed at OMCs/Nafion/GC electrode. The electrocatalytic activity of OMCs/Nafion/GC is ascribed to edge-plane-like defective sites on OMCs [6,10]. In contrast, the Cu_2S/OMCs/Nafion/GC electrode shows an enhanced cathodic response at −0.24 V. The peak potential for reduction of hydrogen peroxide at Cu_2S/OMCs/Nafion/GC is more positive than that at OMCs/Nafion/GC, shifting positively by about 70 mV. The higher reductive current observed from CVs suggests that the hybrid Cu_2S/OMCs catalyst exhibits much better electroreduction activity towards hydrogen peroxide than pristine OMCs. For the bared and Nafion modified GC electrodes, the CVs curve slightly change before and after adding hydrogen peroxide. The comparative result suggests that Cu_2S nanoparticles on the OMCs matrix facilitate the electrochemical reduction of hydrogen peroxide. The improved electrocatalytic performance of Cu_2S/OMCs/Nafion/GC is ascribed to the following three possible reasons. First, OMCs matrix with high specific surface area acts as a good support for achieving a high dispersion of Cu_2S nanoparticles and therefore a high catalytic activity. Second, the accessible mesopores of Cu_2S/OMCs nanocomposite provide sufficient room for hydrogen peroxide to transport to electrode surface. Third, the Cu_2S/OMCs heterostructures provide a favorable microenvironment to shuttle electron between hydrogen peroxide and the working electrode, thus greatly enhance the electron transfer reaction of hydrogen peroxide. The combination of three possible reasons above contributes to the excellent electrocatalytic reduction of hydrogen peroxide at the Cu_2S/OMCs/Nafion/GC electrode.

3.3. Amperometric response to hydrogen peroxide on Cu_2S/OMCs/Nafion/GC electrode

Fig. 6 shows the CA of Cu_2S/OMCs/Nafion/GC with successive additions of hydrogen peroxide at the potential of −0.10 V. The Cu_2S/OMCs/Nafion/GC exhibits fast response to the addition of hydrogen peroxide. The Cu_2S/OMCs/Nafion/GC electrode achieves 95% of the steady-current in 3.6 s. Such a fast response could be attributed to the excellent electroreduction activity of

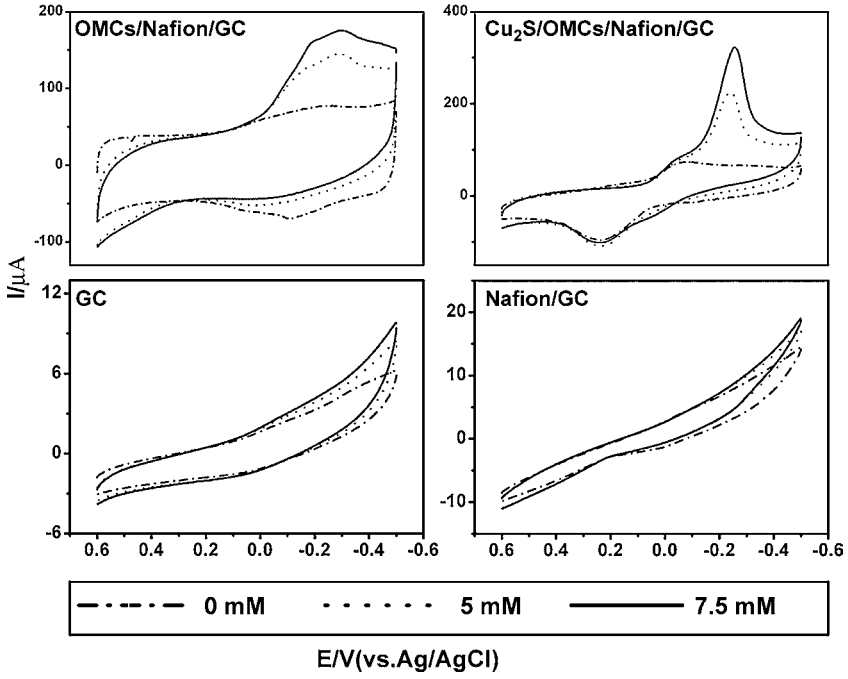

Fig. 5. CVs obtained in 0.1 M PBS (pH 7.3) containing 0 mM (dash dot line), 5 mM (dot line), and 7.5 mM (solid line) hydrogen peroxide at OMCs/Nafion/GC, Cu_2S/OMCs/Nafion/GC, GC, and Nafion/GC electrodes.

Table 2
Comparison of the performance of various hydrogen peroxide sensors based on cathodic measurement schemes.

Electrode	Linear range (μM)	Detection limit (μM) (S/N = 3)	Response time (s)	Potential applied (V)	Reference
Hb/SA[a]–MWCNTs[b]/GC	40–200	16.41	10	−0.40 (vs. SCE)	[35]
Ti(III)–TNTs[c]/Hb	4.9–1100	1.5	<5	−0.10 (vs. SCE)	[45]
(PSS[d]/HRP)$_5$/ZnO/Au	5–1700	2.1	<5	−0.25 (vs. SCE)	[46]
(PDDA[e]/Fe_3O_4)$_5$/ITO[f]	4.18–800	1.4	3.5	−0.20 (vs. Ag/AgCl)	[47]
HRP–Nafion–SPE[g]	5.98–35.36	0.48	–	−0.35 (vs. SCE)	[56]
ZnO/Au/Nafion/HRP/GC	15–1100	9	5	−0.30 (vs. Ag/AgCl)	[57]
Cu_2S/OMCs/Nafion/GC	1–3030	0.2	3.6	−0.10 (vs. Ag/AgCl)	This work

[a] Sodium alginate.
[b] Multiwall carbon nanotubes.
[c] TiO_2 nanotubes in situ self-doped with Ti(III).
[d] Poly(sodium 4-styrenesulfonate).
[e] Poly(diallyldimethylammonium chloride).
[f] Tin-doped indium oxide.
[g] Screen-printed electrode.

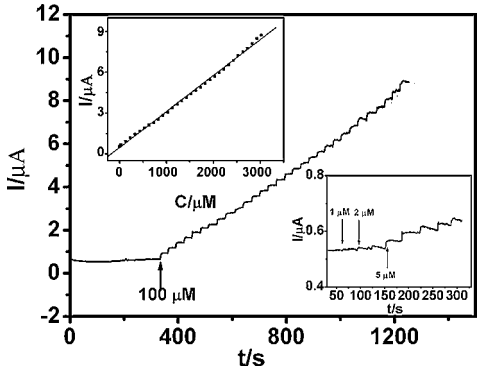

Fig. 6. CA of Cu_2S/OMCs/Nafion/GC to successive additions of hydrogen peroxide at the potential of −0.10 V. Right inset shows the amplification of current–time response to 1, 2, and 5 μM hydrogen peroxide. Left inset shows the corresponding calibration plots for Cu_2S/OMCs/Nafion/GC electrode.

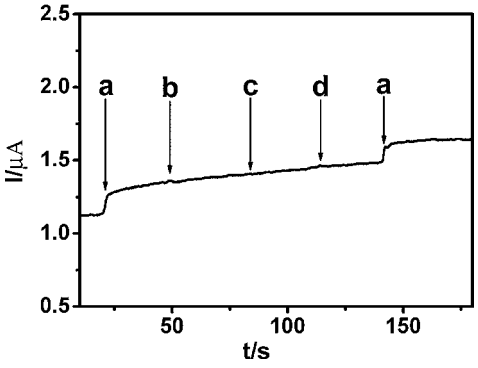

Fig. 7. CA of Cu_2S/OMCs/Nafion/GC to successive additions of (a) 50 μM hydrogen peroxide, (b) 50 μM AA, (c) 50 μM UA, and (d) 50 μM DA at the potential of −0.10 V.

Cu_2S nanoparticles towards hydrogen peroxide and rapid diffusion of hydrogen peroxide inside the mesopores of OMCs. The Cu_2S/OMCs/Nafion/GC electrode has linear chronoamperometric responses to hydrogen peroxide concentrations between 1 and 3030 μM (R = 0.9986, n = 38). The sensitivity is calculated as 36.8 μA mM^{-1} cm^{-2}. The detection limit is 0.2 μM with the signal to noise ratio of three. A comparison of linear range, detection limit, response time, and detection potential for Cu_2S/OMCs nanocomposite modified electrode with other hydrogen peroxide sensors reported in the literature is shown in Table 2. All the data reveal the analytical parameters for Cu_2S/OMCs/Nafion/GC electrode are comparable and even better than those obtained at several electrodes reported recently. Therefore, the Cu_2S/OMCs nanocomposite is a good electrode material for preparation of low detection potential, prompt response, and wide linear range amperometric sensor for hydrogen peroxide determination.

3.4. Influence of interference, stability and reproducibility

In real sample, some electroactive species such as ascorbic acid (AA), uric acid (UA), and dopamine (DA) might affect the determination of hydrogen peroxide. Here, we investigated the interference effect of AA, UA, and DA towards the determination of hydrogen peroxide in Fig. 7. There is obvious current response with the addition of 50 μM hydrogen peroxide (a). On the contrary, no obvious current response is observed with the addition of 50 μM AA (b), UA (c), and DA (d). The good ability of anti-interference is attributed to the low potential. And also in the neutral solution AA exists as a negatively charged species. The absent signal of AA at Cu_2S/OMCs/Nafion/GC electrode can be explained by considering that the negatively charged Nafion repulses the negatively charged ascorbate anions. This hydrogen peroxide sensor was also used to evaluate the feasibility of hydrogen peroxide determination in serum samples. The samples were diluted 20 times with 0.1 M PBS (pH 7.3). By using a standard addition method, the recoveries of hydrogen peroxide samples with concentrations of 0.10 mM (sample 1) and 0.50 mM (sample 2) were obtained. Table 3 shows the calculated recovery values. The results show that this new electrode has a potential use in nonenzymatic detection of hydrogen peroxide.

When the Cu_2S/OMC/Nafion/GC electrode was stored at 4 °C for 3 weeks, the current response to 2 mM hydrogen peroxide remained 91% of its original value, suggesting the long-term stability of the electrode. The reproducibility of the sensor was also investigated. The relative standard deviation (RSD) for 2 mM hydrogen peroxide sensing was <8.1% for five measurements for the same electrode.

Table 3
Determination of hydrogen peroxide in serum sample solutions (n = 4).

	Found (mM)	Added (mM)	After added (mM)	RSD (%)	Mean recovery (%)
Sample 1	0.017	0.10	0.113	3.4	96.0
Sample 2	0.015	0.50	0.501	2.9	97.2

4. Conclusion

A new in situ growth method has been developed to synthesize new Cu_2S/OMCs nanocomposite with Cu_2S nanoparticles embedded inside the pores of OMCs matrix. In application to electrochemistry, the Cu_2S/OMCs nanocomposite exhibits excellent electrocatalytic activity towards hydrogen peroxide. The Cu_2S/OMCs/Nafion/GC also shows negligible interference for AA, UA, and DA. The fast response, wide linear range, and simple preparation process make the Cu_2S/OMCs nanocomposite promising for being developed as a nonenzymatic hydrogen peroxide sensor.

Acknowledgement

The authors gratefully acknowledge the financial support by the National Natural Science Foundation of China (No. 20875012).

References

[1] R. Ryoo, S.H. Joo, S. Jun, J. Phys. Chem. B 103 (1999) 7743–7746.
[2] M. Zhou, J. Ding, L.P. Guo, Q.K. Shang, Anal. Chem. 79 (2007) 5328–5335.
[3] J.C. Ndamanisha, J. Bai, B. Qi, L. Guo, Anal. Biochem. 386 (2009) 79–84.
[4] G. Hu, Y. Guo, S. Shao, Biosens. Bioelectron. 24 (2009) 3391–3394.
[5] L. Zhu, C. Tian, D. Yang, X. Jiang, R. Yang, Electroanalysis 20 (2008) 2518–2525.
[6] M. Zhou, L. Shang, B. Li, L. Huang, S. Dong, Electrochem. Commun. 10 (2008) 859–863.
[7] M. Zhou, L.P. Guo, Y. Hou, X.J. Peng, Electrochim. Acta 53 (2008) 4176–4184.
[8] Y. Hou, L. Guo, G. Wang, J. Electroanal. Chem. 617 (2008) 211–217.
[9] D. Zheng, J. Ye, L. Zhou, Y. Zhang, C. Yu, J. Electroanal. Chem. 625 (2009) 82–87.
[10] N. Jia, Z. Wang, G. Yang, H. Shen, L. Zhu, Electrochem. Commun. 9 (2007) 233–238.
[11] G. Hu, Y. Ma, Y. Guo, S. Shao, J. Electroanal. Chem. 633 (2009) 264–267.
[12] A. Stein, Z. Wang, M.A. Fierke, Adv. Mater. 21 (2009) 265–293.
[13] C. Liang, Z. Li, S. Dai, Angew. Chem. Int. Ed. 47 (2008) 3696–3717.
[14] S. Zhu, H. Zhou, M. Hibino, I. Honma, M. Ichihara, Adv. Funct. Mater. 15 (2005) 381–386.
[15] Y. Wang, L. Cheng, F. Li, H. Xiong, Y. Xia, Chem. Mater. 19 (2007) 2095–2101.
[16] Y. Hou, J.C. Ndamanisha, L. Guo, X. Peng, J. Bai, Electrochim. Acta 54 (2009) 6166–6171.
[17] Y. Sun, L. Zhuang, J. Lu, X. Hong, P. Liu, J. Am. Chem. Soc. 129 (2007) 15465–15467.
[18] W.C. Choi, S.I. Woo, M.K. Jeon, J.M. Sohn, M.R. Kim, H.J. Jeon, Adv. Mater. 17 (2005) 446–451.
[19] H. Lee, S.W. Yoon, E.J. Kim, J. Park, Nano Lett. 7 (2007) 778–784.
[20] J. Chen, S.Z. Deng, N.S. Xu, S. Wang, X. Wen, S. Yang, C. Yang, J. Wang, W. Ge, Appl. Phys. Lett. 80 (2002) 3620–3622.
[21] Y. Myung, D.M. Jang, Y.J. Cho, H.S. Kim, J. Park, J.U. Kim, Y. Choi, C.J. Lee, J. Phys. Chem. C 113 (2009) 1251–1259.
[22] L. Chen, Y. Xia, X. Liang, K. Yin, J. Yin, Z. Liu, Y. Chen, Appl. Phys. Lett. 91 (2007) 073511–073513.
[23] F. Gao, Q. Lu, D. Zhao, Chem. Phys. Lett. 360 (2002) 585–591.
[24] W.-H. Zhang, X.-B. Lu, J.-H. Xiu, Z.-L. Hua, L.-X. Zhang, M. Robertson, J.-L. Shi, D.-S. Yan, J.D. Holmes, Adv. Funct. Mater. 14 (2004) 544–552.
[25] W. Xu, Y. Liao, D.L. Akins, J. Phys. Chem. B 106 (2002) 11127–11131.
[26] Z. Zhang, S. Dai, X. Fan, D.A. Blom, S.J. Pennycook, Y. Wei, J. Phys. Chem. B 105 (2001) 6755–6758.
[27] Y. Shan, L. Gao, Mater. Chem. Phys. 89 (2005) 412–416.
[28] W.H. Zhang, J.L. Shi, H.R. Chen, Z.L. Hua, D.S. Yan, Chem. Mater. 13 (2001) 648–654.
[29] K. Dimos, I.B. Koutselas, M.A. Karakassides, J. Phys. Chem. B 110 (2006) 22339–22345.
[30] F. Gao, Q. Lu, X. Liu, Y. Yan, D. Zhao, Nano Lett. 1 (2001) 743–748.
[31] S. Hanaoka, J.M. Lin, M. Yamada, Anal. Chim. Acta 426 (2001) 57–64.
[32] X. Yang, Y. Guo, Z. Mei, Anal. Biochem. 393 (2009) 56–61.
[33] N. Jie, J. Yang, X. Huang, R. Zhang, Z. Song, Talanta 42 (1995) 1575–1579.
[34] C. Matsubara, N. Kawamoto, K. Takamura, Analyst 117 (1992) 1781–1784.
[35] H.Y. Zhao, W. Zheng, Z.X. Meng, H.M. Zhou, X.X. Xu, Z. Li, Y.F. Zheng, Biosens. Bioelectron. 24 (2009) 2352–2357.
[36] J.W. Shie, U. Yogeswaran, S.M. Chen, Talanta 78 (2009) 896–902.
[37] A.K. Upadhyay, T.W. Ting, S.M. Chen, Talanta 79 (2009) 38–45.
[38] F. Xi, L. Liu, Z. Chen, X. Lin, Talanta 78 (2009) 1077–1082.
[39] Y. Liu, Q. Xu, X. Feng, J.J. Zhu, W. Hou, Anal. Bioanal. Chem. 387 (2007) 1553–1559.
[40] Z. Dai, S. Liu, H. Ju, H. Chen, Biosens. Bioelectron. 19 (2004) 861–867.
[41] J.J. Feng, J.J. Xu, H.Y. Chen, Biosens. Bioelectron. 22 (2007) 1618–1624.
[42] N. Jia, Y. Wen, G. Yang, Q. Lian, C. Xu, H. Shen, Electrochem. Commun. 10 (2008) 774–777.
[43] C. You, X. Yan, J. Kong, D. Zhao, B. Liu, Electrochem. Commun. 10 (2008) 1864–1867.
[44] A. Salimi, R. Hallaj, S. Soltanian, Biophys. Chem. 130 (2007) 122–131.
[45] M. Liu, G. Zhao, K. Zhao, X. Tong, Y. Tang, Electrochem. Commun. 11 (2009) 1397–1400.
[46] B.X. Gu, C.X. Xu, G.P. Zhu, S.Q. Liu, L.Y. Chen, M.L. Wang, J.J. Zhu, J. Phys. Chem. B 113 (2009) 6553–6557.
[47] L. Zhang, Y. Zhai, N. Gao, D. Wen, S. Dong, Electrochem. Commun. 10 (2008) 1524–1526.
[48] B. Zhao, Z. Liu, Z. Liu, G. Liu, Z. Li, J. Wang, X. Dong, Electrochem. Commun. 11 (2009) 1707–1710.
[49] M.R. Guascito, E. Filippo, C. Malitesta, D. Manno, A. Serra, A. Turco, Biosens. Bioelectron. 24 (2008) 1057–1063.
[50] L. Zhang, H. Li, Y. Ni, J. Li, K. Liao, G. Zhao, Electrochem. Commun. 11 (2009) 812–815.
[51] J.C. Ndamanisha, Y. Hou, J. Bai, L. Guo, Electrochim. Acta 54 (2009) 3935–3942.
[52] J. Bai, B. Qi, J.C. Ndamanisha, L. Guo, Micropor. Mesopor. Mater. 119 (2009) 193–199.
[53] D. Zhao, J. Feng, Q. Huo, N. Melosh, G.H. Fredrickson, B.F. Chmelka, G.D. Stucky, Science 279 (1998) 548–552.
[54] S. Jun, S.H. Joo, R. Ryoo, M. Kruk, M. Jaroniec, Z. Liu, T. Ohsuna, O. Terasaki, J. Am. Chem. Soc. 122 (2000) 10712–10713.
[55] B. Marler, U. Oberhagemann, S. Vortmann, H. Gies, Micropor. Mater. 6 (1996) 375–383.
[56] Y.J. Teng, S.H. Zuo, M.B. Lan, Biosens. Bioelectron. 24 (2009) 1353–1357.
[57] C. Xiang, Y. Zou, L.-X. Sun, F. Xu, Sens. Actuators B 136 (2009) 158–162.